Supplemental Information Inventory

Supplemental Figures

Figure S1.

Both the "closed" to "open" transition, as well as Wts activity, depend on the capacity of Wts to be bound by Mats (related to Figure 1).

Q ratio images are shown for CWT (**A**) and CWT^{R708A} (**B**), the latter a version of CWT mutated for a conserved Arginine required for Wts to be bound by Mats (expressed under control of the *Tubα1* promoter in *wts*^{X1}/+ discs). Both sets of images were identically imaged, processed, and scaled (color scale as in Fig. 2). Note the characteristic central to peripheral increase in Q for wild type CWT, in contrast to the uniform high Q values for CWT^{R708A}. The *Tubα1.CWT* transgene fully rescues Wts function in *wts*^{X1}/*wts*^{X1} animals in contrast to *Tubα1.CWT*^{R708A} transgene, which is

devoid of rescuing activity, indicating that Wts must be bound by Mats to adopt the "open" state and become active.

Figure S2.

Apical membrane accumulation and conformation of the CWT-Wts sensor is not polarized, in contrast to Dachs (related to Figure 2).

A) A wing disc peppered with small clones expressing either Dachs-GFP (green), the Wts-CWT sensor (orange), or both, imaged for Dachs-GFP and CWT protein accumulation is shown on the left panel (clones expressing both appear green as the Dachs-GFP signal predominates; the wing primordium is outlined with a dotted line and the proximo-distal axes indicated). The regions in boxes 1 through 5 are shown magnified on the right, together with the corresponding Q ratio image (color scale above; Dachs-GFP is not apparent (deep blue) in the Q ratio image as emission in the acceptor channel approaches zero for GFP). Apical Dachs-GFP accumulates predominately on the distal edge of each cell, as can be seen by comparing Dachs-GFP signal on the distal versus the proximal edges of each clone. No such proximo-distal bias is apparent for either Wts-CWT accumulation or Q ratios.

B) Average signal intensities along the proximal and distal edges of individual clones were measured for CWT accumulation, and separately Dachs-GFP accumulation (as diagramed on top), and the distal/proximal ratios of signal intensity displayed on in the boxplots on the left: the individual ratios determined for each clone are shown as black diamonds; the boxes display both the median (horizontal lines through the box) and interquartile range (tops and bottoms of the boxes). Median measurements are: 1.05 for CWT abundance, and 1.76 for mEGFP-Dachs abundance. For the CWT clones we also determined the average Q ratios for the distal and the proximal interfaces of each clone. The results are displayed on the right using the same boxplot format as on the left. Both the median and interquartile range of the Q ratio values obtained for the distal edges appear statistically indistinguishable from those obtained for the proximal edges. For comparison, we performed the same analysis on the average Q ratios for apical cell interfaces from *wildtype* (*w.t.*) as well as neighboring $ds^{-}ft^{-}$ tissue – specifically from cell-cell interfaces within clone "a" in Fig. S4 versus interfaces in the *wildtype* surround. In this case the difference in Q is unequivocal, providing a positive control for our capacity to see differences in Q that normally correlate with physiologically relevant differences in the level of "closed" versus "open" CWT. P values less or equal to 0.001 are indicated by three red stars.

Figure S3.

Clones singly mutant for either *ds* or *ft* behave like *ds*$^{-}$*ft*$^{-}$ double mutant clones, showing levels of increased CWT-sensor activity (Q) that correlate with the extent of the reduction in Wts activity (related to Figure 3).

A, B) Q ratio images of the apical surface of two wing discs containing *ds*$^{-}$ clones (the center panels show the Q ratio images with the clone borders annotated in white; the left panels show the unannotated images, and the right panels show the clones marked by the expression of myristoylated RFP (mRFP)). The clones appear red relative to the green surround.

C, D) Q ratio images of the apical surface of two wing discs containing *ft*$^{-}$ clones (annotated and marked as in **A**, **B**). The clones appear redder relative to the green surround than the *ds*$^{-}$ clones (**A**, **B**), correlating with the more severe reduction in Wts activity caused by the removal of Ft compared to Ds.

Figure S4.

Loss of both Ft and Ds causes a shift in the CWT sensor from the "open" to the "closed" conformation, correlating with reduced Wts activity but independent of changes in the stability of the CWT sensor (related to Figure 3).

A, B) Q ratio image (**A**) of the apical surface of a wing disc containing numerous *ds*$^{-}$*ft*$^{-}$ clones marked by the expression of mRFP (white in **B**), some outlined in yellow, turquoise or purple, and others not outlined (Q scaled as in Fig. 2). The clones appear red relative to the green surround, with sharp red/green interfaces at the clone borders, indicating a cell autonomous difference in conformational state of the CWT Wts-FRET sensor. Note that two clones of large squamous cells in the overlying peripodial cell layer are apparent above the columnar epithelium **B** (but not **A**), just below, and to the right, of the clone marked "a".

C) Corresponding acceptor channel image of the same disc, with intensity proportional to the amount of CWT protein. For *ds*$^{-}$*ft*$^{-}$ clones, the level of apical CWT varies from clone to clone, sometimes being similar to the level in neighboring cells (*e.g.,* clone "a", outlined in turquoise), and sometimes being significantly lower (e.g., clone "b" outlined in purple).

D) Box graph showing Q measurements derived from 10 cellular interfaces located either within *ds*$^{-}$*ft*$^{-}$ clone "a" or "b", or in the corresponding *wildtype* cells that neighbor these clones (horizontal line through the box indicates the mean, and the tops and bottoms of the boxes indicate the third and the first quartiles, respectively). A similar differential in Q between the clone and the surround is observed for both clones,

irrespective of the apparent difference in CWT stability (similar to the surround for “a”, and reduced relative to the surround for “b”).

E) Z stacks and projections of corresponding acceptor and donor channel images from a representative *ds*$^{-}$*ft*$^{-}$ clone. Z-stack images (top row, acceptor channel; middle rows, donor channels with and without annotation; bottom row, clone marked by mRFP) for a *ds*$^{-}$*ft*$^{-}$ clone (clone “a” from Fig. S4) are shown starting with the most apical section on the left (note the clone in the overlying squamous peripodial cell layer). The last column shows the maximal projection of the individual focus planes, with the Q ratio image shown for the annotated donor channel. Note that there is a slight Z-displacement of the acceptor and donor channel images for any given focal plane owing to uncorrected chromatic aberration inherent to the objective – this displacement is averaged out in the maximum projection.

Figure S5.

Wts conformational state, as monitored by the CWT sensor, is not altered by the absence of either Hpo kinase, or Expanded, an upstream facilitator of Hpo kinase activity (related to Figure 6).

A, B, C) Q ratio images of the apical surface of wing discs containing numerous *hpo*$^{-}$ clones (as in Fig. S3, the left and middle panels show the unannotated and annotated Q images, and the right panels show the clone marker, mRFP; the orange box indicates the region containing a *hpo*$^{-}$ clones shown at high magnification in Fig. 6B). Despite the presence of the clones, the discs show the stereotyped Q ratio pattern characteristic of *wildtype* discs, with a progressive green to red shift in the distal to proximal direction, as well as increased green versus red signal in the vicinities of the A/P and D/V compartment boundaries (e.g., Fig. 2). The lack of effect on Q ratios observed in *hpo*$^{-}$ clones is in marked contrast to the abrupt increase of Q ratios in *mats*,$^{-}$ *ds*$^{-}$*ft*$^{-}$*, ds*$^{-}$*,* and *ft*$^{-}$ clones (appear red; Figs. 1, 3, S3, S4), even though all of these mutant conditions reduce (*ds*$^{-}$*ft*$^{-}$*, ds*$^{-}$*, ft*$^{-}$) or abolish (*hpo*$^{-}$, *mats*$^{-}$) Wts activity.

D, E) Q ratio images of the apical surface of two wing discs, each containing numerous *ex*$^{-}$ clones (as in Fig. S3, the left and middle panels show the unannotated and annotated Q images, and the right panels show the clone marker, mRFP; only clones in the columnar cell layer, and not the overlying periopodial cell layer are annotated in the middle panels). Both discs show the stereotyped Q ratio pattern characteristic of *wildtype* discs (e.g., Fig. 2), except that some of the clones appear slightly greener than the *wildtype* surround, despite the fact that *ex* null clones have reduced Wts activity.

Figure S6.

RNAi knock-down of Mats and Ft, but not Hpo or Ex, causes an increase in CWT sensor activity (Q) (related to Figure 6).

Apical Q ratio images are shown for wing discs that express RNAi's targeting *mats*, *ft*, *ex*, or *hpo* transcripts in the posterior (p) compartment under en.Gal4 control. Although all four genotypes cause the wings of adult flies to have abnormally large p compartments (not shown), indicating that the RNAi's are effective at knocking down their target transcripts and, as a consequence, compromising Wts activity, only Mats and Ft knock-down cause an increase in Q ratios (the p compartment appears redder than the anterior compartment (a), whereas the Ex and Hpo knock-down do not (a and p compartments appears similarly green).

Figure S7.

Removal of Dachs causes a shift of Wts from the "closed" to the "open" conformation even when Hpo activity is compromised by a reduction in Ex activity (related to Figures 5 and 6).

A,B) Q ratio images of the apical surface of two wing discs, both homozygous for ex^{Z} (also called ex^{697}), a hypomorphic allele of *ex*, and each containing clones of d^{-} cells (as in Fig. S3, the left and middle panels show the unannotated and annotated Q images, and the right panels show the clone marker, mRFP). ex^{Z} discs show excessive wing growth due to reduced Hpo function, irrespective of whether they retain or lack Dachs function. Hence, the reduction in Wts activity resulting from reduced Ex-dependent phosphorylation of Wts by Hpo is epistatic to (i.e., downstream and independent of) the normal requirement for Dachs. Nevertheless, d^{-} clones in ex^{Z} discs exhibit a decrease in Q ratio (appear greener than the surround). Because the decrease in Q caused by the removal of Dachs depends on Mats (Fig. 5E), we infer that Mats can enrich the "open" state sensor population even when Hpo activity is compromised by reduced Ex function. These results corroborate our findings with hpo- and ex- clones (Figs. 6B, S5, and S6) that the capacity of Mats to regulate the conformational state of Wts, as monitored by the CWT sensor, does not depend on the phosphorylation of either Wts or Mats by Hpo.

Figure S8.

Control of Wts conformation by Ft/Ds signaling does not depend on the capacity of Wts to auto-phosphorylate itself (related to Figure 6).

A,B) Apical Q ratio images of wts^{X1}/+ wing discs carrying clones of $ds^{-}ft^{-}$ cells, and expressing CWT^{K749R}, a mutant form of the CWT Wts sensor that is devoid of kinase activity (**A**), or CWT^{S920A}, a mutant form that lacks the Serine residue that is the likely target of auto-phosphorylation (**B**). As in Fig. S3, the left and middle panels show the

unannotated and annotated Q images, and the right panels show the clone marker, mRFP (only clones in the columnar epithelia are visible and annotated in the Q ratio images). In both cases, clones appear red relative to the *wildtype* surround, indicating an increase in occupancy in the “closed” state, as observed for the *wildtype* CWT sensor (Fig. 3A), even though neither sensor can undergo auto-phosphorylation.

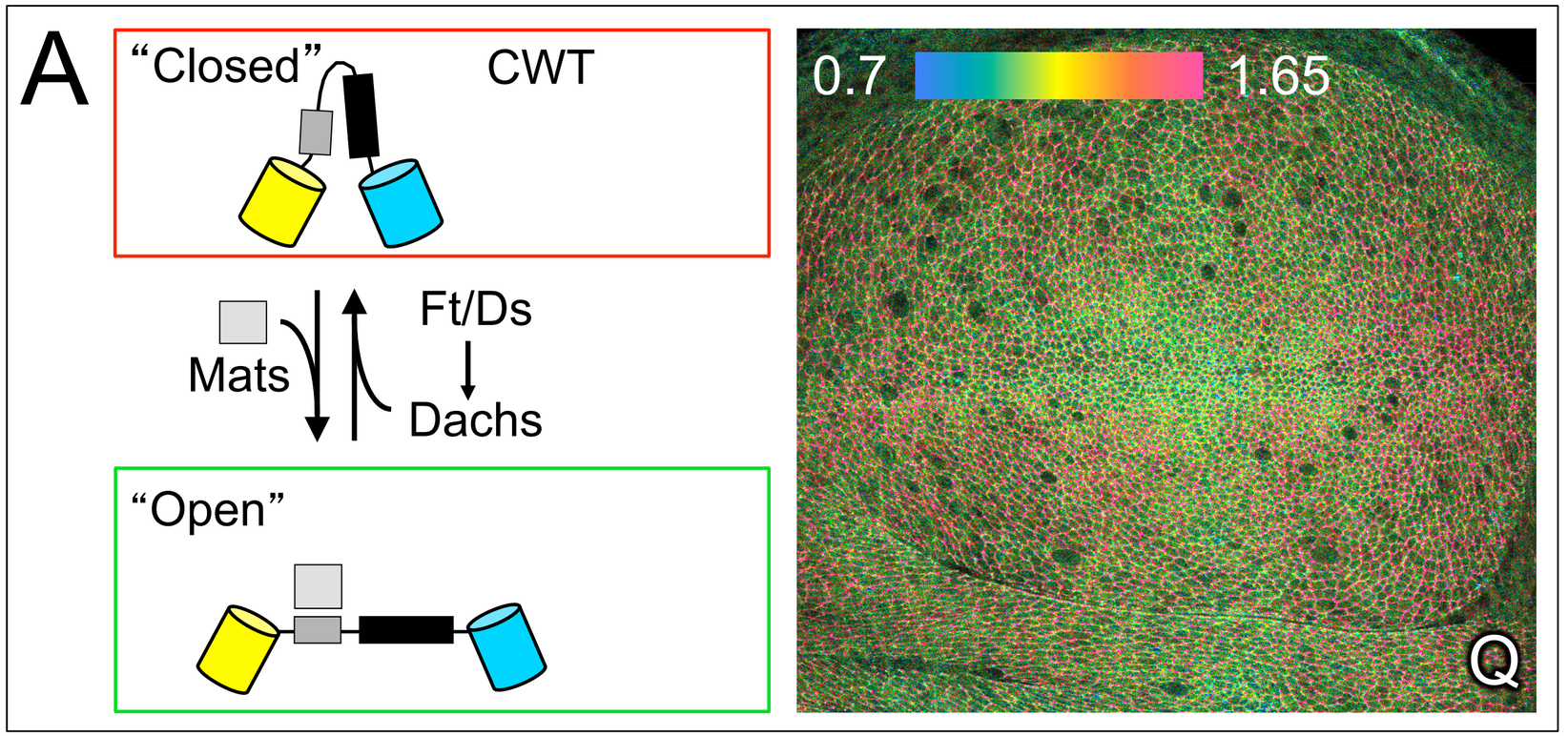

Vrabioiu and Struhl
Figure S1

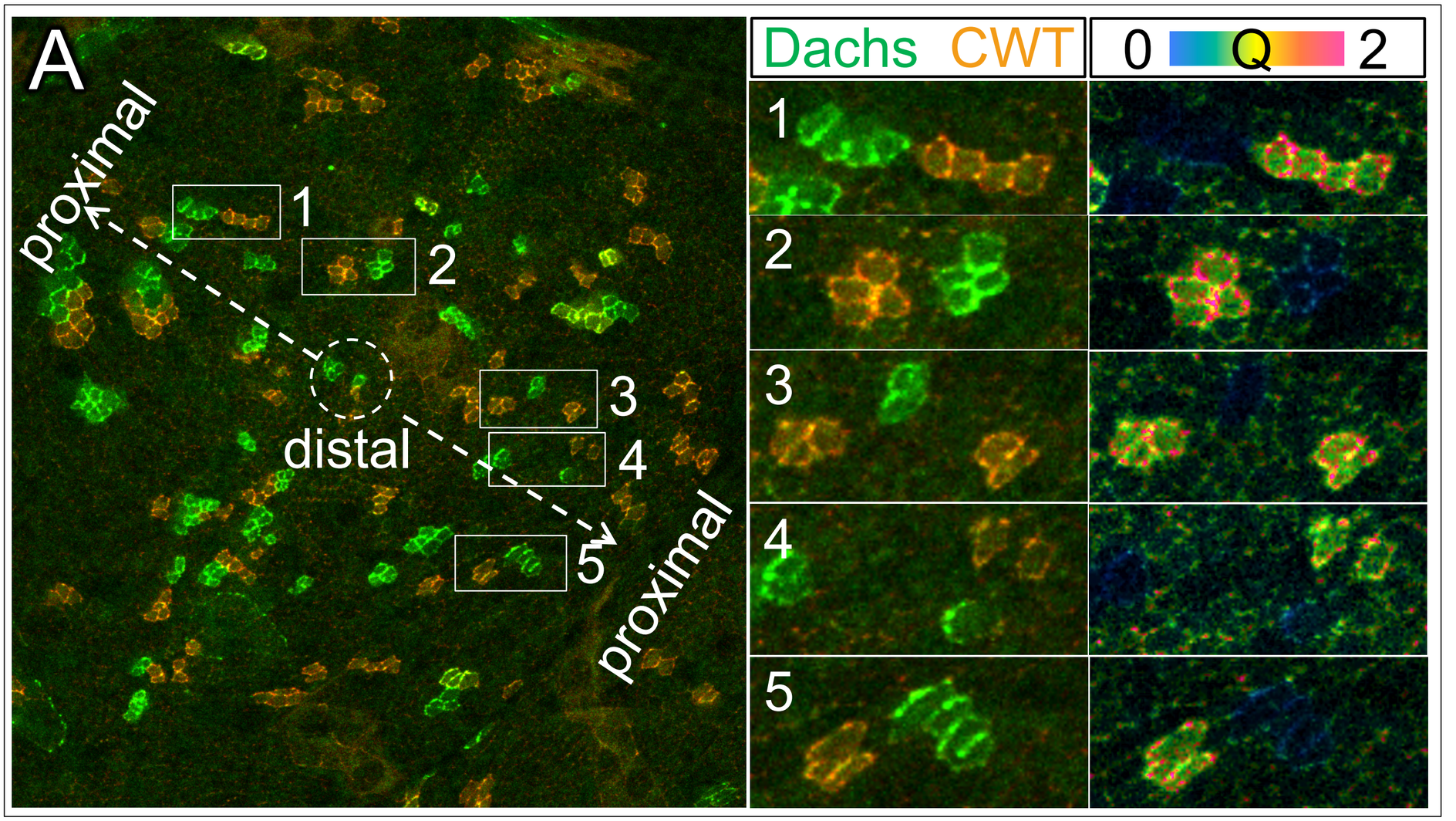

Vrabioiu and Struhl, Figure S2

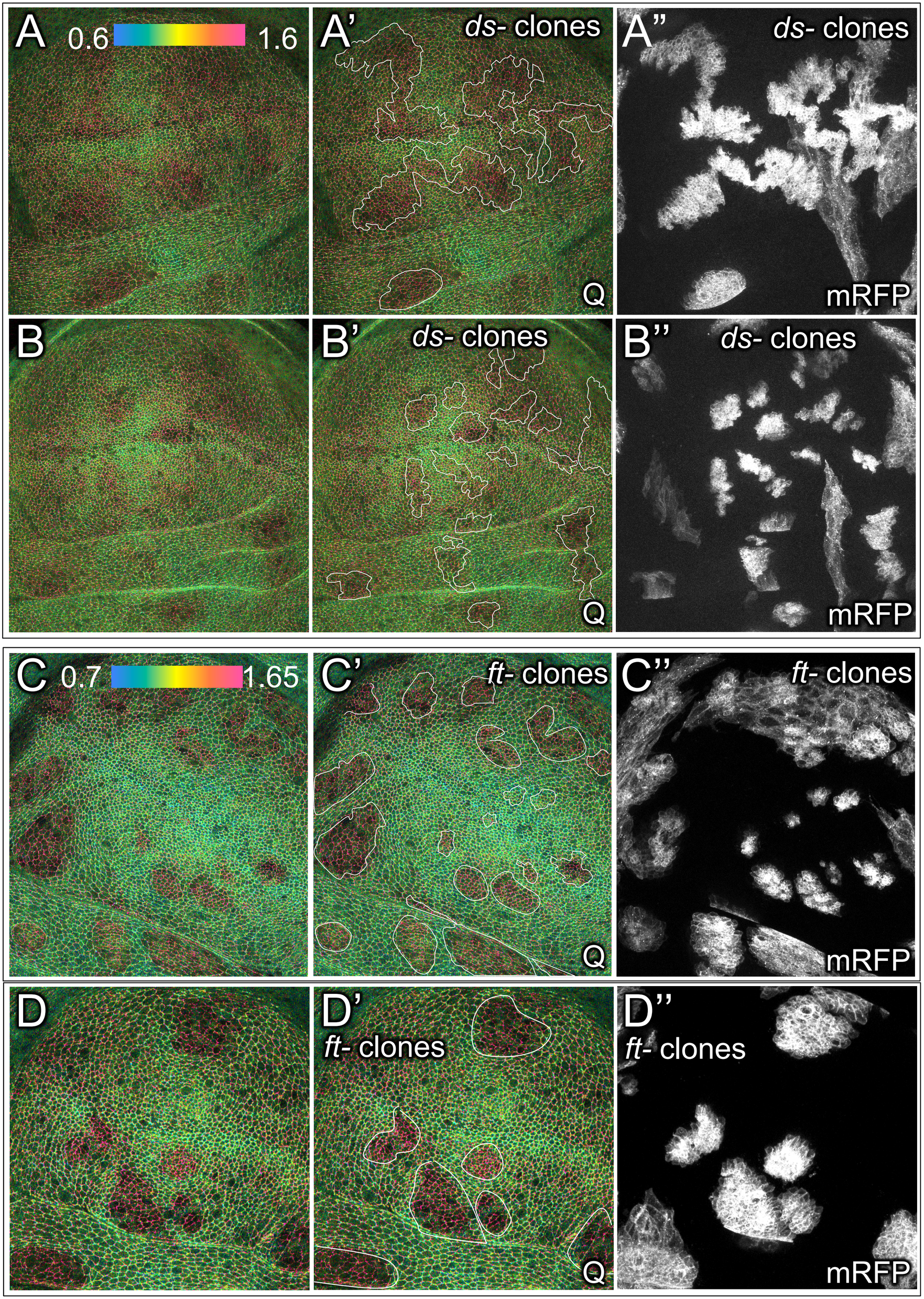

Vrabioiu and Struhl, Figure S3

A

ds-ft- clones

b

a

Q

B

ds-ft- clones

b

a

mRFP

C

ds-ft- clones

b

a

CWT

D

a

CWT

w.t. = ds- ft-

b

CWT

w.t. > ds- ft-

Q

3.0

2.5

2.0

1.5

1.0

w.t

ds-ft-

w.t

ds-ft-

E

Apical

Baso-lateral

Projection

Acceptor

Donor

Donor

mRFP

Q

Vrabioiu and Struhl, Figure S4

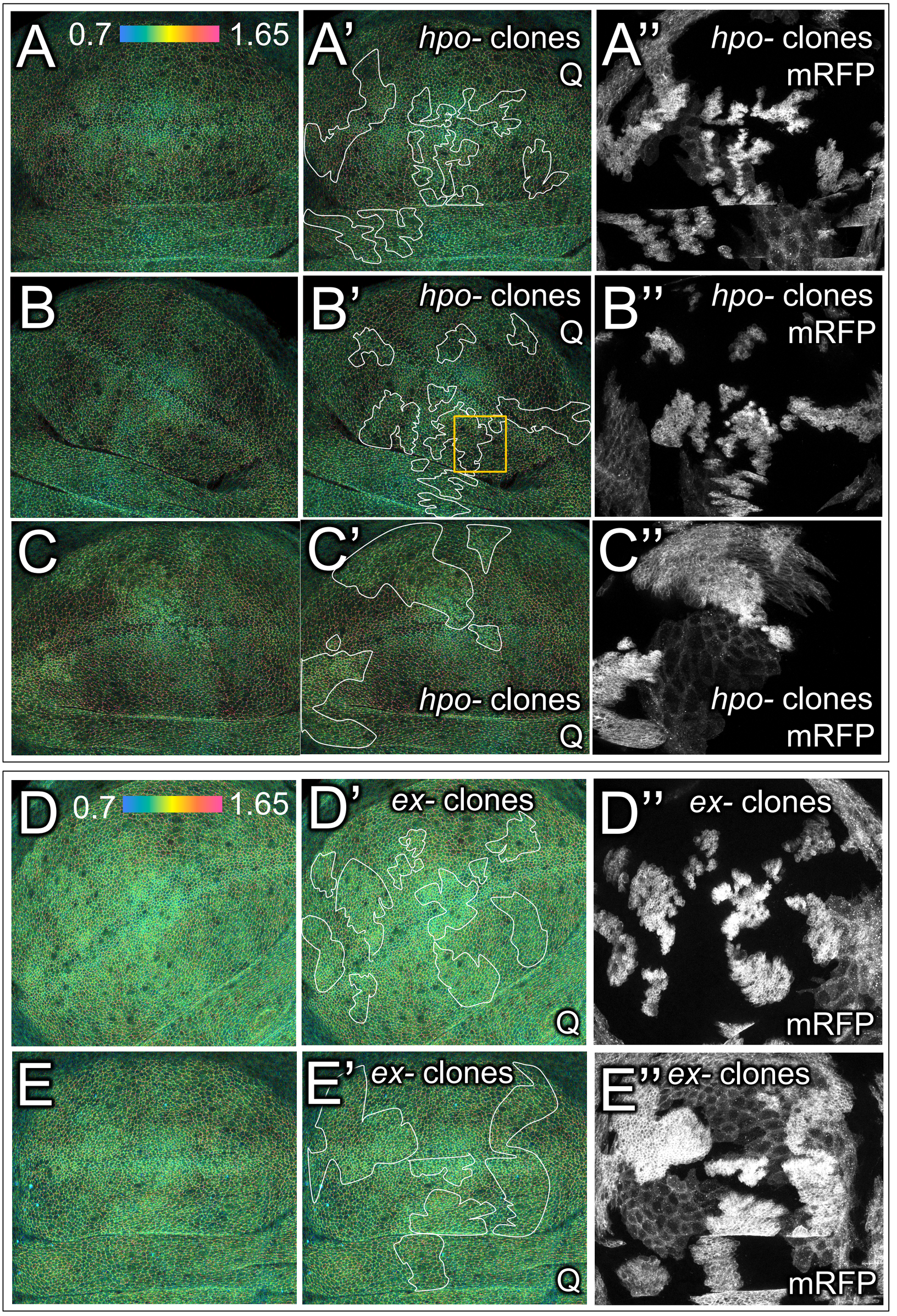

Vrabioiu and Struhl, Figure S5

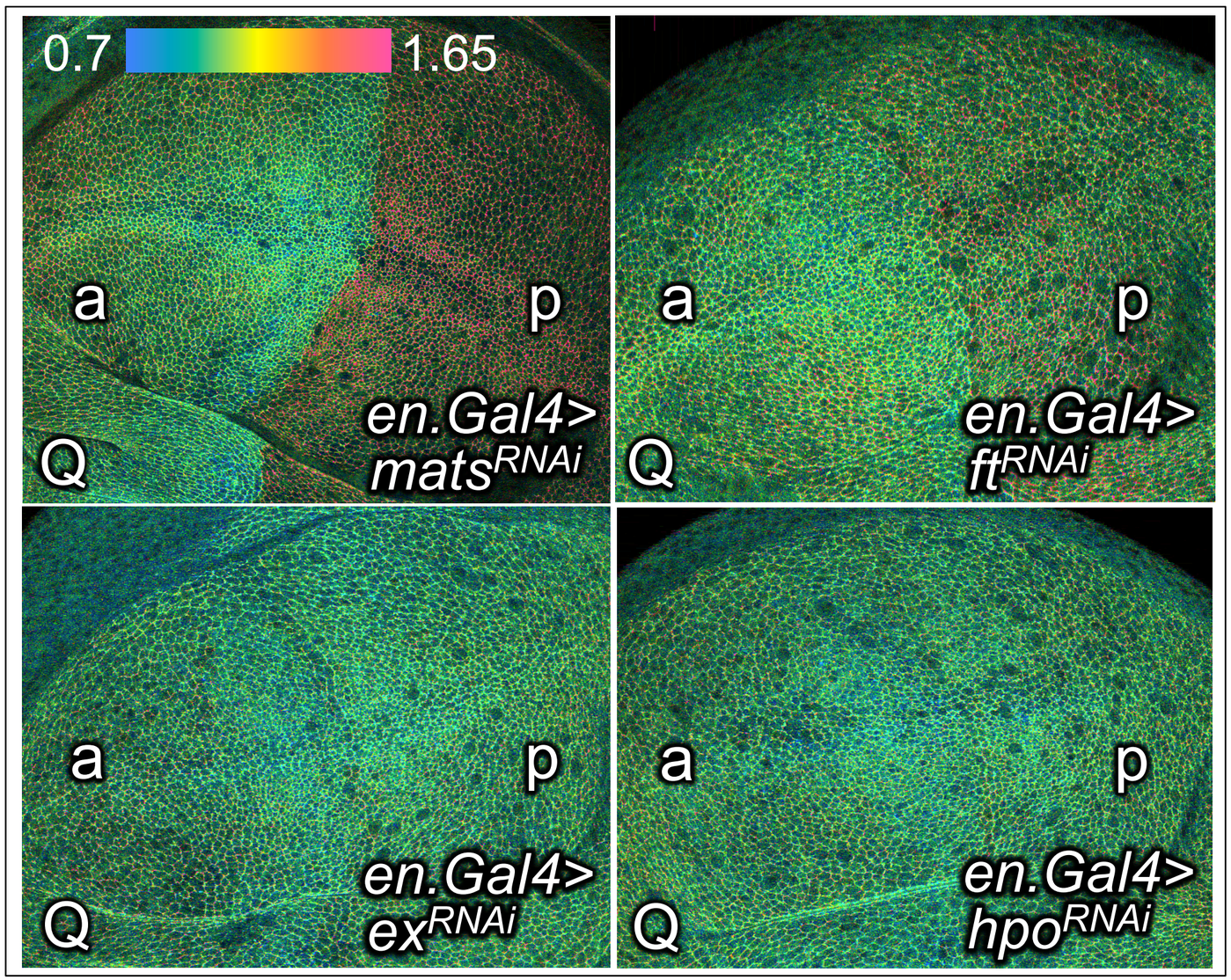

Vrabioiu and Struhl, Figure S6

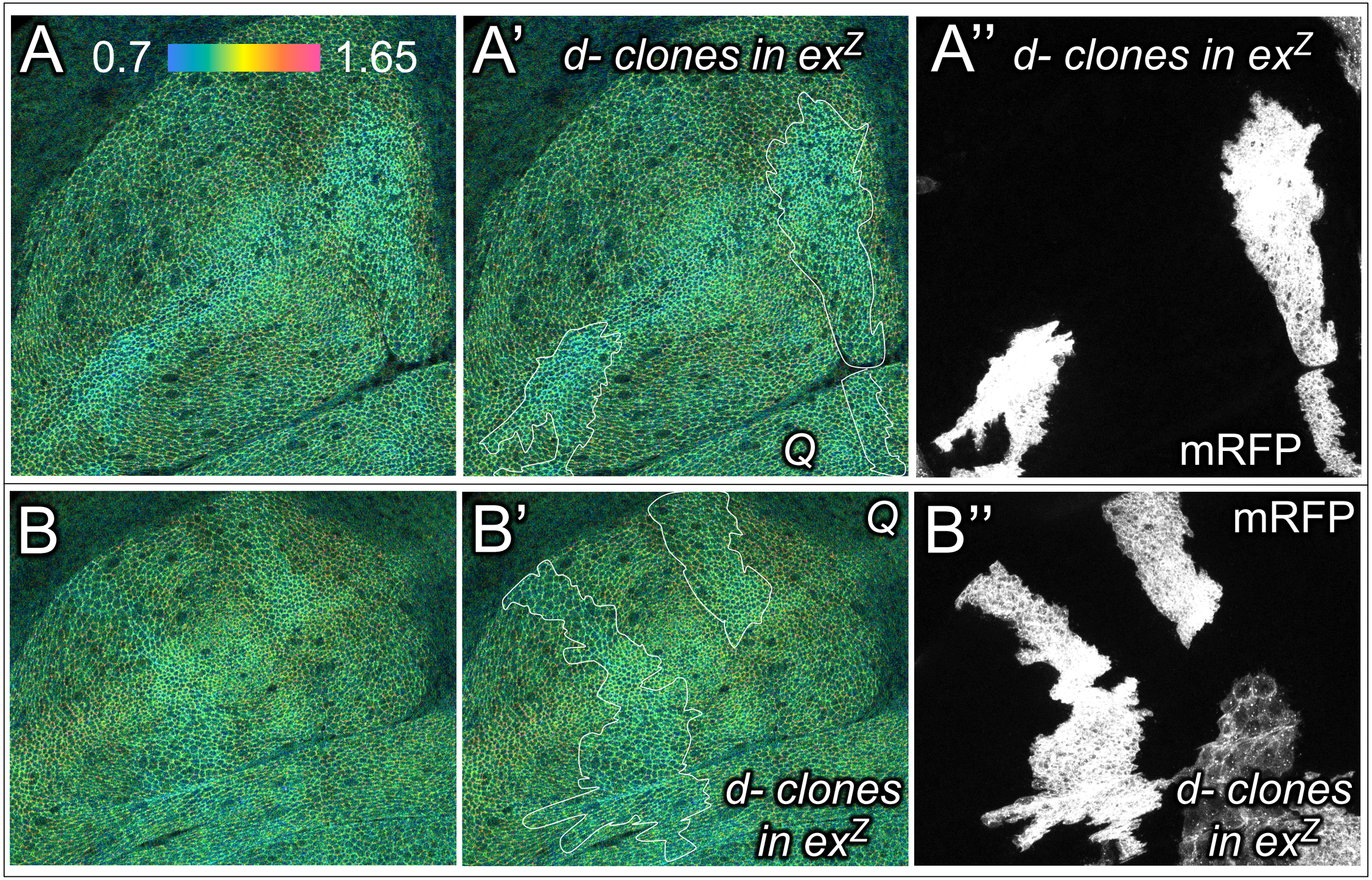

Vrabioiu and Struhl, Figure S7

A

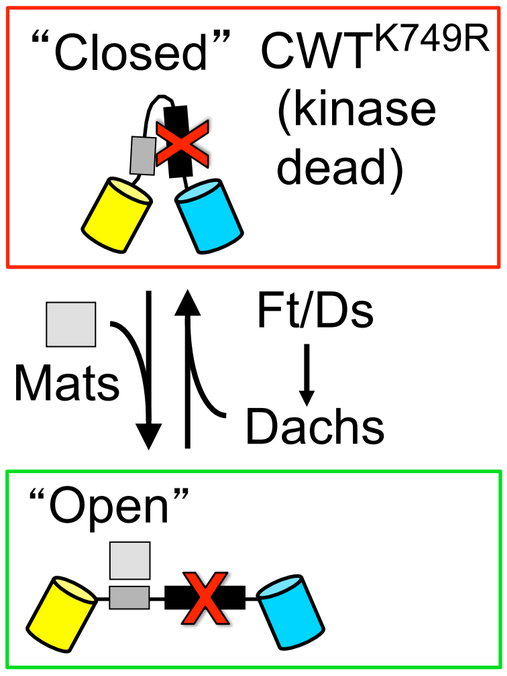

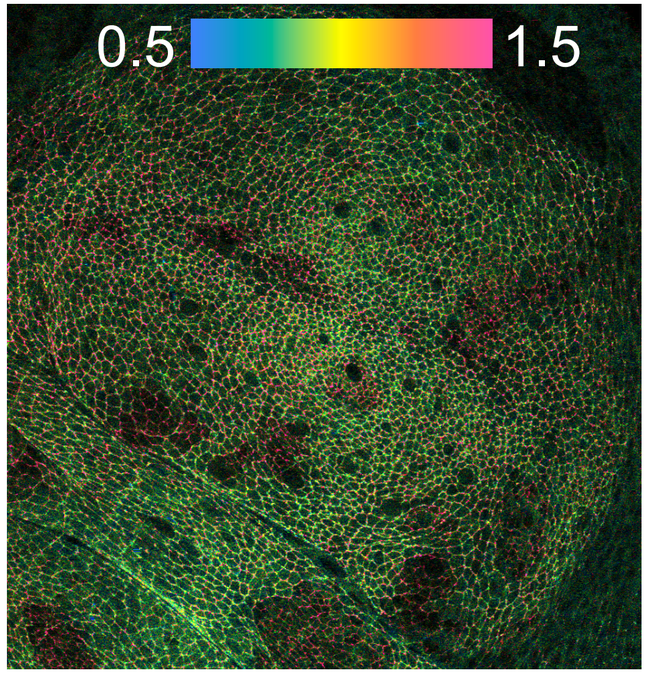

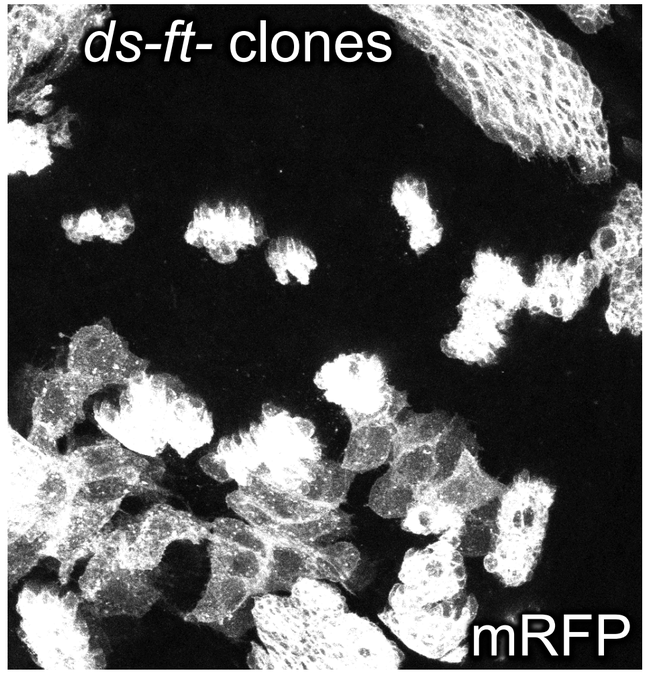

B

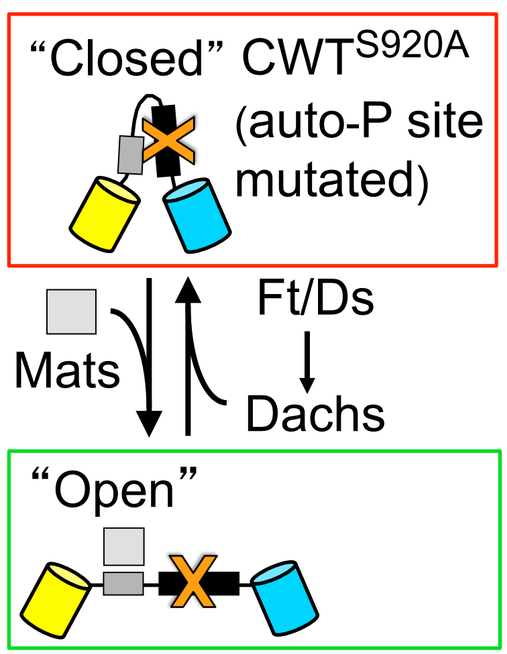

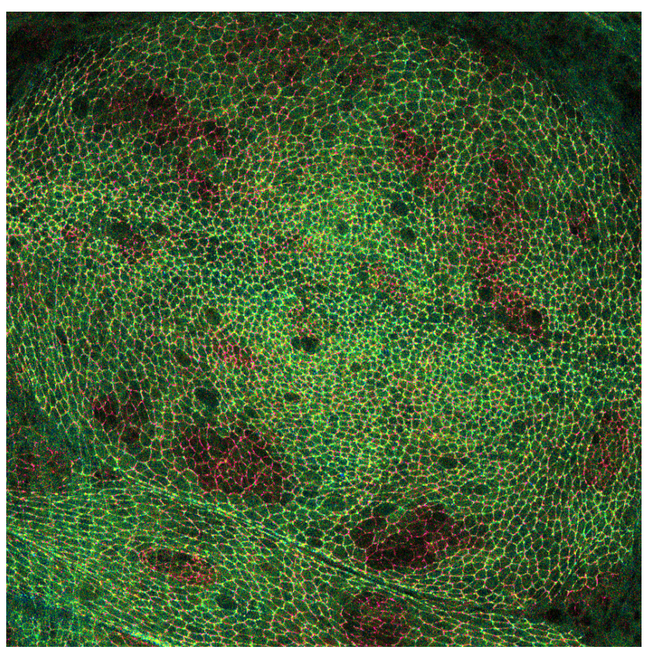

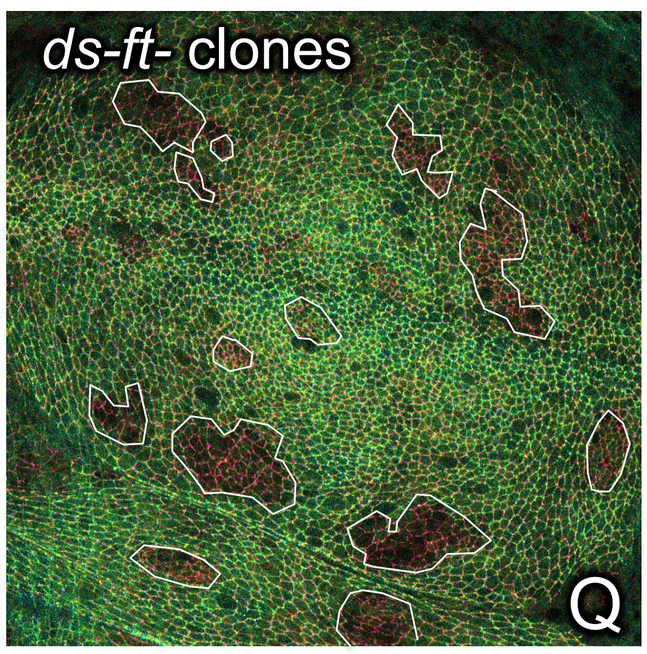

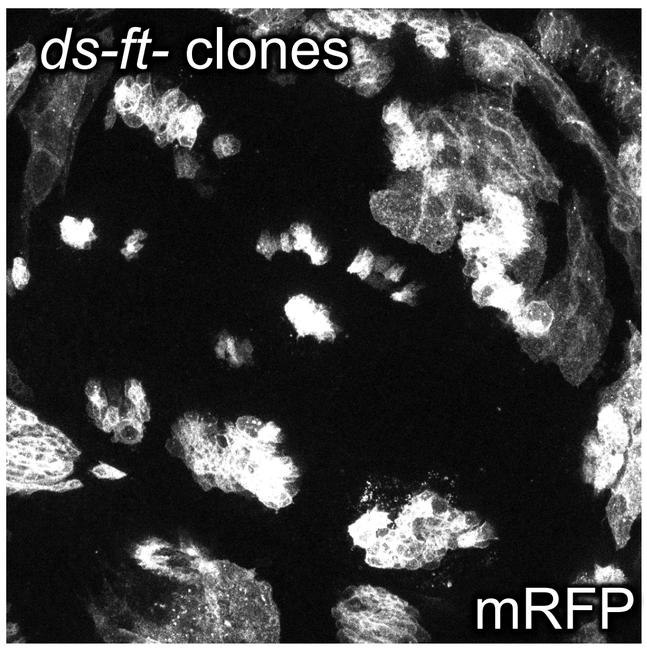

Vrabioiu and Struhl, Figure S8

Extended Experimental Procedures

Wild type and mutant CWT FRET sensor coding sequences.

We based construction of our CWT and TWC FRET sensors on the wts coding sequence as annotated in Flybase (http://flybase.org/). *CWT*^{T1083A} encodes a mutant version of CWT in which the sole Threonine residue phosphorylated by Hpo (Emoto et al., 2006) is replaced with Alanine. *CWT*^{R708A} encodes a mutant version of CWT in which the Arginine residue predicted to be essential for Mats binding (Hergovich et al., 2006a; Ni et al., 2015) is mutated to Alanine. *CWT*^{K749R} encodes a mutant version of CWT in which the Lysine residue predicted to be essential for kinase activity (Hanks et al., 1988; Xia et al., 2002) is mutated to Arginine. *CWT*^{S920A} encodes a CWT version in which a conserved Serine implicated as the target site for Wts auto-phosphorylation (Hergovich et al., 2006b) is mutated to Alanine.

Generation of transgenes expressing CWT and TWC Wts-FRET sensors at physiological levels in the developing wing imaginal disc.

Transgenic flies expressing the CWT and TWC coding sequences under the transcriptional control of the *Tubulin*α*1* (*Tub*α*1*) and *ribosomal protein 49* (*rp49*) promoters were generated as in (Basler and Struhl, 1994; Greenwood and Struhl, 1997). For the *Tub*α*1* transgenes, the promoter was initially separated from the coding sequence by a *>CD2, y*^{2}*>* Flp-out cassette [as in (Casali and Struhl, 2004)]. In single copy, all of the *rp49>CWT* and *Tub*α*1>CWT* transgenes (except for *Tub*α*1>CWT*^{T1083A}, *Tub*α*1>CWT*^{R708A} *Tub*α*1>CWT*^{K749A}, and *Tub*α*1>CWT*^{S920A}) rescue the lethality of *wts*^{X1} null homozygotes, producing viable, phenotypically normal, fertile adults. Real time PCR data indicates that the *rp49>CWT* transgene is expressed at ~1-2X the level of endogenous *wts*, while the *Tub*α*1>CWT* transgene is expressed ~2-4X higher than endogenous *wts*. For reference, overexpression of *wts* coding sequences such as *CWT* under *Tub*α*1.Gal4/UAS* control results in 20-40X the level of endogenous *wts* expression and causes animal lethality. Conversely, the *>CD2, y*^{2}*>* Flp-out cassette does not abolish transcription of the downstream *CWT* coding sequence in the *Tub*α*1>CD2, y*^{2}*>CWT* transgene, but instead reduces it ~ 5 fold to a level that generally fails to rescue *wts*^{X1} mutant animals to adulthood. Thus the levels of CWT expression generated under *rp49>* and *Tub*α*1>* control are in the physiologically normal range. Similar results were obtained with the *rp49>CWT*

and *Tubα1>CWT* transgenes, although the two fold higher level of expression of the *Tubα1* transgene provided a better signal to noise ratio.

Generation of transgenes for expressing tagged forms of Mats, Ft and Ds under Gal4/UAS control.

ft-mCherry, *mCherry-mats*, *ds-mCherry*, and *mEGFP-d* coding sequences were assembled as follows: Ft coding sequence (Mahoney et al., 1991) was fused at its 3' end to the coding sequence for mCherry (linked by SLGSGSGGGAG), the Mats coding sequence (Lai et al., 2005) was fused at its 5' end to the mCherry coding sequence via GAPSGTGGS, and mCherry sequence, flanked by an N-terminal GRASGGGSGG peptide linker and C-terminal GLNPR peptide linker was inserted downstream of the transmembrane domain of Ds (just after MRSRKPR). Dachs coding sequence (dD isoform, http://flybase.org/) was fused at its 5' end to the mEGFP coding sequence via a GAPGGSGGS peptide linker. The *ft*, *mats*, and *ds* coding sequences were introduced into a standard *pUAST* vector containing an attB site and inserted into a docking site at 86Fb (Brand and Perrimon, 1993; Bischof et al., 2007). Dachs coding sequence was inserted downstream of a *>CD2, y*$^{+}$> Flp-out cassette, to generate the sequence *Tubα1>CD2,y*$^{+}$*>mEGFP-d* in an attB vector that was further inserted into the docking site at 86Fb.

Drosophila mutations and transgenes

The following alleles were used: *wts*^{X1}, *mats*^{e03077}, *hpo*$^{5.1}$ (Genevet et al., 2009), *ft*$^{G\text{-}Rv}$, *ft*^{15}, *ds*^{071}, *ds*$^{GS.D}$ (*UAS.ds*), *d*^{GC13}, *ex*^{697}, *ex*^{e1} (http://flybase.org/). In addition, a new Dachs null allele (*d*^{V}) lacking the entirety of the major *d* transcript [*d-RD* (http://flybase.org/)] was made using FRT mediated recombination of the Exelixis lines f07701 and c03443 (Thibault et al., 2004; Bellen et al., 2011). Homozygous *d*^{V} adults appeared indistinguishable from *d*^{GC13} adults.

UAS.myrRFP and *UAS.yki-V5* (Oh and Irvine, 2009) transgenes were obtained from the Bloomington stock collection. Standard *Tubα1.Gal4*, *Tubα1.Gal80*, and *hsp70.flp* transgenes were used to generate clones of cells marked by the expression of myristoylated RFP (see Experimental genotypes, below). The RNAi stocks were obtained from VDRC (http://stockcenter.vdrc.at/; #102550 for *d*^{RNAi}) and Bloomington *Drosophila* Stock Center (http://flystocks.bio.indiana.edu/; TRIP.HMS01096 for *d*^{RNAi}, TRIP.HMS00475 for *mats*^{RNAi}, TRIP.HMS00874 for *ex*^{RNAi}, TRIP.HMS00006 for *hpo*^{RNAi}, TRIP.HMS00932 for *ft*^{RNAi}).

Unless otherwise indicated, all experiments assaying the conformational state of the CWT and TWC sensors were performed in *wts* null mutant animals, with the

Tubα1>wts or *rp49>wts* transgenes providing the only source of functional Wts protein.

Experimental genotypes

***Tubα1>CWT* discs**

y w hsp70.flp; Tubα1>CWT wts^{X1}/wts^{X1}

***Tubα1>CWT* discs in *wts* heterozygous background**

y w hsp70.flp; Tubα1>CWT wts^{X1}/+

***Tubα1> CWT*^{R708A} discs in *wts* heterozygous background**

y w hsp70.flp; Tubα1> CWT^{R708A} wts^{X1}/+

***Tubα1> CWT* clones in *Tubα1>CD2, y*^{2}*>CWT* discs**

y w hsp70.flp; Tubα1>CD2, y^2*>CWT/*wts^{X1}

Tubα1> CWT* and *Tubα1>mEGFP-dachs clones

y w hsp70.flp; Tubα1>CD2, y^2*>CWT* wts^{X1}*/ Tubα1>CD2, y*$^+$*>mEGFP-dachs*

***rp49>CWT* discs**

y w hsp70.flp; rp49>CWT wts^{X1}/wts^{X1}

***mats*^{e03077} clones in *rp49>CWT* discs**

y w hsp70.flp; tubα1.Gal4 UAS.myrRFP/Sp or *CyO; rp49>CWT* $mats^{e03077}$ wts^{X1}*/rp49>CWT tub.Gal80* wts^{X1}

***mats* knock down in the posterior compartment using RNAi**

y w hsp70.flp; en.Gal4/Sp or *CyO; Tubα1>CWT* wts^{X1}*/UAS.*$mats^{RNAi}$

***ft*$^-$ clones in *Tubα1>CWT* discs**

y w hsp70.flp; ft^{15} *FRT39/Tubα1.Gal80 FRT39; Tubα1>CWT* wts^{X1}*/Tubα1.Gal4 UAS.myrRFP* wts^{X1}

***ds*$^-$ clones in *Tubα1>CWT* discs**

y w hsp70.flp; ds^{UA071} *FRT39/Tubα1.Gal80 FRT39; Tubα1>CWT* wts^{X1}*/Tubα1.Gal4 UAS.myrRFP* wts^{X1}

_ds⁻ ft⁻_ clones in _Tubα1>CWT_ discs

y w hsp70.flp; ds^{UA071} ft^{15} FRT39/Tubα1.Gal80 FRT39; Tubα1>CWT wts^{X1}/Tubα1.Gal4 UAS.myrRFP wts^{X1}

_ds⁻ ft⁻_ clones in _Tubα1>TWC_ discs

y w hsp70.flp; ds^{UA071} ft^{15} FRT39/Tubα1.Gal80 FRT39; Tubα1>TWC wts^{X1}/Tubα1.Gal4 UAS.myrRFP wts^{X1}

UAS.ds clones in _Tubα1>CWT_ discs

y w hsp70.flp; $ds^{GS.D}$ UAS.myrRFP/CyO; Tubα1>CWT Tubα1>w^{+}>Gal4 wts^{X1}/wts^{X1}

y w hsp70.flp; Tubα1>CWT Tubα1>w^{+}>Gal4 wts^{X1}/UAS.ds-mCherry wts^{X1}

UAS.ft clones in _Tubα1>CWT_ discs

y w hsp70.flp; Tubα1>CWT Tubα1>w^{+}>Gal4 wts^{X1}/UAS.ft-mCherry wts^{X1}

_d_ knock down in clones using RNAi

y w hsp70.flp; UAS.myrRFP/Sp or *CyO; Tubα1>CWT Tubα1>w+>Gal4 wts^{X1}/UAS.d^{RNAi}* (TRIP.HMS01096)

_d_ knock down in the posterior compartment using RNAi

y w hsp70.flp; en.Gal4/Sp or *CyO; Tubα1>CWT wts^{X1}/UAS.d^{RNAi}* (VDRC # 102550)

_d⁻_ clones in _Tubα1>CWT_ discs

y w hsp70.flp; d^{GC13} FRT39/Tubα1.Gal80 FRT39; Tubα1>CWT wts^{X1}/Tubα1.Gal4 UAS.ykiV5 UAS.myrRFP wts^{X1}

y w hsp70.flp; stc FRT39/Tubα1.Gal80 FRT39; Tubα1>CWT wts^{X1}/Tubα1.Gal4 UAS.ykiV5 UAS.myrRFP wts^{X1}

d⁻ Tubα1>CWT discs

y w hsp70.flp; d^{GC13}; Tubα1>CWT wts^{X1}/wts^{X1}

UAS.ft or _UAS.ds_ clones in _d⁻ Tubα1>CWT_ discs

y w hsp70.flp; d^{GC13}; Tubα1>CWT Tubα1>w^{+}>Gal4 wts^{X1}/UAS.ft-mCherry wts^{X1}

y w hsp70.flp; d^{GC13}; Tubα1>CWT Tubα1>w^{+}>Gal4 wts^{X1}/UAS.ds-mCherry wts^{X1}

<u>*UAS.mats* clones in *Tubα1>CWT* discs</u>

y w hsp70.flp; Tubα1>CWT Tubα1>w^{+}>Gal4 wts^{X1}/UAS.mCherry-mats wts^{X1}

<u>*$mats^{e03077}$* clones in *d^{-} rp49>CWT* discs</u>

y w hsp70.flp; Tubα1.Gal4 UAS.myrRFP d^{v}/d^{GC13}; rp49>CWT $mats^{e03077}$ wts^{X1}/rp49>CWT Tubα1.Gal80 wts^{X1}

<u>*ds^{-} ft^{-}* clones in *Tubα1> CWT^{T1083A}* discs</u>

y w hsp70.flp; ds^{071} ft^{44} FRT39/Tubα1.Gal80 FRT39; Tubα1>CWT^{T1083A} wts^{X1}/Tubα1.Gal4 UAS.myrRFP

<u>*hpo^{-}* clones in *Tubα1>CWT* discs</u>

y w hsp70.flp; FRT42 $hpo^{5.1}$/FRT42 Tubα1.Gal80; Tubα1>CWT wts^{X1}/Tubα1.Gal4 UAS.myrRFP wts^{X1}

<u>*ex^{-}* clones in *Tubα1>CWT* discs</u>

y w hsp70.flp; ex^{e1} FRT39, ap/Tubα1.Gal80 FRT39; Tubα1>CWT wts^{X1}/Tubα1.Gal4 UAS.myrRFP wts^{X1}

<u>*d^{-}* clones in *ex^{697} Tubα1>CWT* discs</u>

y w hsp70.flp; ex^{697} d^{GC13} FRT39/ ex^{697}Tubα1.Gal80 FRT39; Tubα1>CWT wts^{X1}/Tubα1.Gal4 UAS.myrRFP wts^{X1}

<u>Reduction of *hpo*, *ex*, and *ft* levels in the posterior compartment of *Tubα1>CWT* discs</u>

y w hsp70.flp; en.Gal4, UAS.myrRFP/Sp or *CyO; Tubα1>CWT wts^{X1}/UAS.(hpo, ex, or ft)^{RNAi}*

<u>*ds^{-} ft^{-}* clones in *Tubα1> CWT^{K749R}* discs</u>

y w hsp70.flp; ds^{071} ft^{44} FRT39/Tubα1.Gal80 FRT39; Tubα1>CWT^{K749R} wts^{X1}/Tubα1.Gal4 UAS.myrRFP

<u>*ds^{-} ft^{-}* clones in *Tubα1> CWS^{S920A}* discs</u>

y w hsp70.flp; ds^{071} ft^{44} FRT39/Tubα1.Gal80 FRT39; Tubα1>CWT^{S920A} wts^{X1}/Tubα1.Gal4 UAS.myrRFP

Supplemental References

Basler, K., and Struhl, G. (1994). Compartment boundaries and the control of Drosophila limb pattern by hedgehog protein. Nature *368*, 208-214.

Bellen, H.J., Levis, R.W., He, Y., Carlson, J.W., Evans-Holm, M., Bae, E., Kim, J., Metaxakis, A., Savakis, C., Schulze, K.L.*, et al.* (2011). The Drosophila gene disruption project: progress using transposons with distinctive site specificities. Genetics *188*, 731-743.

Bischof, J., Maeda, R.K., Hediger, M., Karch, F., and Basler, K. (2007). An optimized transgenesis system for Drosophila using germ-line-specific phiC31 integrases. Proc Natl Acad Sci USA *104*, 3312-3317.

Brand, A.H., and Perrimon, N. (1993). Targeted gene expression as a means of altering cell fates and generating dominant phenotypes. Development *118*, 401-415.

Casali, A., and Struhl, G. (2004). Reading the Hedgehog morphogen gradient by measuring the ratio of bound to unbound Patched protein. Nature *431*, 76-80.

Emoto, K., Parrish, J.Z., Jan, L.Y., and Jan, Y.N. (2006). The tumour suppressor Hippo acts with the NDR kinases in dendritic tiling and maintenance. Nature *443*, 210-213.

Genevet, A., Polesello, C., Blight, K., Robertson, F., Collinson, L.M., Pichaud, F., and Tapon, N. (2009). The Hippo pathway regulates apical-domain size independently of its growth-control function. J Cell Sci *122*, 2360-2370.

Greenwood, S., and Struhl, G. (1997). Different levels of Ras activity can specify distinct transcriptional and morphological consequences in early Drosophila embryos. Development *124*, 4879-4886.

Hanks, S.K., Quinn, A.M., and Hunter, T. (1988). The protein kinase family: conserved features and deduced phylogeny of the catalytic domains. Science *241*, 42-52.

Hergovich, A., Schmitz, D., and Hemmings, B.A. (2006a). The human tumour suppressor LATS1 is activated by human MOB1 at the membrane. Biochemical and biophysical research communications *345*, 50-58.

Hergovich, A., Stegert, M.R., Schmitz, D., and Hemmings, B.A. (2006b). NDR kinases regulate essential cell processes from yeast to humans. Nature reviews Molecular cell biology *7*, 253-264.

Lai, Z.-C., Wei, X., Shimizu, T., Ramos, E., Rohrbaugh, M., Nikolaidis, N., Ho, L.-L., and Li, Y. (2005). Control of cell proliferation and apoptosis by mob as tumor suppressor, mats. Cell *120*, 675-685.

Mahoney, P.A., Weber, U., Onofrechuk, P., Biessmann, H., Bryant, P.J., and Goodman, C.S. (1991). The fat tumor suppressor gene in Drosophila encodes a novel member of the cadherin gene superfamily. Cell *67*, 853-868.

Ni, L., Zheng, Y., Hara, M., Pan, D., and Luo, X. (2015). Structural basis for Mob1-dependent activation of the core Mst-Lats kinase cascade in Hippo signaling. Genes Dev *29*, 1416-1431.

Oh, H., and Irvine, K.D. (2009). In vivo analysis of Yorkie phosphorylation sites. Oncogene *28*, 1916-1927.

Thibault, S.T., Singer, M.A., Miyazaki, W.Y., Milash, B., Dompe, N.A., Singh, C.M., Buchholz, R., Demsky, M., Fawcett, R., Francis-Lang, H.L.*, et al.* (2004). A complementary transposon tool kit for Drosophila melanogaster using P and piggyBac. Nature Genetics *36*, 283-287.

Xia, H., Qi, H., Li, Y., Pei, J., Barton, J., Blackstad, M., Xu, T., and Tao, W. (2002). LATS1 tumor suppressor regulates G2/M transition and apoptosis. Oncogene *21*, 1233-1241.